

Surface disordering and its correlations with properties in argon implanted CR-39 polymer

Cite as: J. Appl. Phys. **109**, 083513 (2011); <https://doi.org/10.1063/1.3573480>

Submitted: 14 July 2010 . Accepted: 28 February 2011 . Published Online: 20 April 2011

Nidhi Shekhawat, Sanjeev Aggarwal, Annu Sharma, S. K. Sharma, S. K. Deshpande, and K. G. M. Nair



View Online



Export Citation

ARTICLES YOU MAY BE INTERESTED IN

[Effect of nitrogen ion implantation on the optical and structural characteristics of CR-39 polymer](#)

Journal of Applied Physics **102**, 063527 (2007); <https://doi.org/10.1063/1.2783887>

[Effect of argon ion implantation on the electrical and dielectric properties of CR-39](#)

AIP Conference Proceedings **1731**, 070030 (2016); <https://doi.org/10.1063/1.4947862>

[Surface ripple evolution by argon ion irradiation in polymers](#)

Journal of Applied Physics **119**, 115303 (2016); <https://doi.org/10.1063/1.4944323>

Lock-in Amplifiers
up to 600 MHz



Surface disordering and its correlations with properties in argon implanted CR-39 polymer

Nidhi Shekhawat,¹ Sanjeev Aggarwal,^{1,a)} Annu Sharma,¹ S. K. Sharma,² S. K. Deshpande,³ and K. G. M. Nair⁴

¹Department of Physics, Kurukshetra University, Kurukshetra 136119, India

²Department of Chemical Engineering, I. I. T. Kanpur, Kanpur 208016, India

³UGC-DAE Consortium for Scientific Research, Mumbai Centre, BARC, Mumbai 400085, India

⁴Materials Science Division, Indira Gandhi Centre for Atomic Research, Kalpakkam 603102, India

(Received 14 July 2010; accepted 28 February 2011; published online 20 April 2011)

The influence of Ar⁺ implantation induced disordering in the surface layers of the CR-39 polymer on its optical properties and surface hardness has been studied. The specimens were implanted at 130 keV to the doses of 5×10^{14} , 1×10^{15} , 1×10^{16} Ar⁺ cm⁻². The structural behavior of the pre- and postimplanted specimens was investigated using UV-Visible, Raman, and x-ray diffraction techniques. Formation of disordered graphitelike structures in the implanted layers of polycarbonate has been observed using Raman and UV-Visible spectroscopy. A significant increase in the value of disorder content (Urbach energy) from 0.77 eV to 1.48 eV and a continuous decline in optical bandgap (from 3.43 eV to 2.32 eV) with increasing implantation dose have been observed. This decrease in optical bandgap has been found to have linear dependence on the increase in the Urbach energy, which points toward the formation of disordered structures in the implanted layers of CR-39 polymer. Further, Knoop microhardness is found to be enhanced by a factor of 7 (at a load of 9.8 mN) after implantation. The possible correlation of the increase in Knoop surface hardness with the changes observed as a result of implantation has been established and discussed. © 2011 American Institute of Physics. [doi:10.1063/1.3573480]

I. INTRODUCTION

Polymers offer unique properties, application prospects, and diversity in performance and characteristics, which cannot be matched by any other class of material. Polymers are extensively used in making optical fibers, optical filters, sensors, lenses, etc., and have immense importance, as they are widely replacing metals in various disciplines. Some polymers are also used in bulletproofing as a result of their high strength.¹⁻³ Yet sometimes their industrial applications are limited by undesirable surface properties like low density, high elasticity, chemical inertness, poor electrical conductivity, low hardness, etc. All these properties of polymers need to be modified without altering their bulk properties.⁴⁻⁶

Interest in ion beam induced improvement in the surface of various polymers has increased in recent years. As the energetic ions used for the modification have limited penetration depth up to a few μm or nm (depending upon their energy and Z) therefore, they can be used for modifying the surface of the polymers without altering the bulk structure. During the ion implantation process, the incident ion loses its energy via nuclear and electronic stopping processes. Nuclear energy loss arises from collisions between the incident ions and the target nuclei causing atomic displacements and phonons, whereas electronic energy loss arises from the interaction between the incident ions and target electrons resulting in electronic excitations and ionizations. All these processes in the target surface lead to the formation of a disordered

network, which contains structural disorders in the form of free radicals, broken chain segments, and dangling bonds.^{7,8}

The implantation of noble gaseous ions eliminates the doping effect of impurities and makes it possible to study the radiation effects of ions on the polymer without bonding with the polymeric chains.^{4,9,10} Therefore, these beams have gathered great attention from researchers, as they can produce far superior products in terms of improved surface hardness, reduced wear, increased corrosion resistance, better biocompatibility, improved optical properties, altered electrical/electronic properties, etc. We have chosen argon ions to modify the surface structure of the CR-39 polymer, basic monomer structure of which is shown in Fig. 1. CR-39 is a transparent, thermosetting resin (aliphatic polycarbonate) that combines an exceptional range of qualities that are not available in other transparent plastic materials. It is used in making lenses, solid-state nuclear track detectors, sensors, photographic filters, etc.¹¹⁻¹³

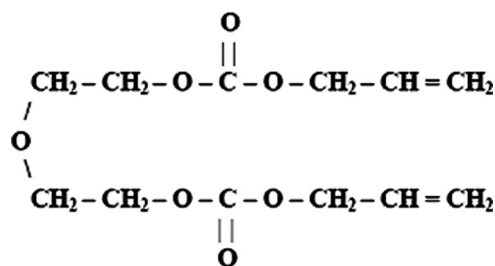


FIG. 1. Monomer structure of CR-39 polymer.

^{a)}Author to whom correspondence should be addressed. Electronic mail: write2sa@gmail.com.

Some reports are present in the literature on similar ion–substrate combinations (but with different ion beam parameters like energy, dose, current, etc.).^{12–16} Yap *et al.* have measured changes in optical and mechanical properties of the CR-39 polymer as an effect of 50 keV argon ion implantation. They have shown a drastic decline in optical bandgap and a nearly five times hike in the nanohardness of the implanted specimens.^{12–14} Abdul-Kader *et al.* have also studied changes in the optical bandgap and Vickers microhardness of the CR-39 polymer after subjecting it to 320 keV argon ion implantation. They have reported a continuous decrease in optical bandgap and a nearly three times enhancement in the microhardness of the implanted specimens.^{15,16} The disordering produced during implantation is largely responsible for such changes in the properties.^{12–16} The measurement of disorder content using the Urbach edge method and the intensity ratio (I_D/I_G) of the D and G bands observed in Raman spectra is an important concept, and has not been addressed clearly in available reports.

The aim of our present work is to study the disorder content in surface layers of the CR-39 polymer as a result of argon ion implantation and to establish correlations with the changes observed in its optical bandgap and surface hardness. The study of microhardness and UV-Visible absorption in implanted specimens provides information regarding change in its strength and energy bandgap. Alteration in the bandgap of implanted specimens enhances the electronic applications of this polymer whereas modifications to the microhardness can improve its application in situations where common polymers suffer mechanical failure due to unwanted conditions. In the present case, we have studied the effect of 130 keV Ar^+ implantation with different ion fluences on the optical bandgap and Knoop microhardness of the CR-39 polymer. The structural and chemical changes as a result of ion implantation have been investigated by using glancing angle X-ray diffraction (GXR), UV-Visible, and Raman spectroscopy. The possible correlations of the disorder parameters with optical bandgap and microhardness have been established and discussed.

II. EXPERIMENTAL DETAILS

$1 \times 1 \text{ cm}^2$ samples were cut from 1 mm thick sheets of optically transparent CR-39 polymer supplied by M/S TAS-TRAK (Bristol, England). Some of these samples were implanted with 130 keV Ar^+ ions under a vacuum of 7.5×10^{-7} Torr, using the 150 kV Linear Accelerator facility available at Materials Science Division, Indira Gandhi Centre of Atomic Research, Kalpakkam, India. A low beam current density of $0.35 \mu\text{A cm}^{-2}$ was used to achieve fluences of 5×10^{14} , 1×10^{15} , and 1×10^{16} ions cm^{-2} . The average range of implanted argon was ~ 180 nm as per Stopping and Range of Ions in Matter (SRIM) simulations. The value of electronic and nuclear losses was 2.66 eV/\AA and 2.70 eV/\AA , respectively.

UV-Visible transmission and absorption studies in the pre- and postimplanted specimens were carried out using Shimadzu Double beam double monochromator spectrophotometer (UV-2550), equipped with Integrated Sphere Assem-

bly ISR-240A in the wavelength range of 190–900 nm with a resolution of 0.5 nm. All absorption spectra were recorded, keeping air as the reference.

The chemical and structural changes as a result of implantation were recorded using a Wi Tec, Confocal Micro-Raman Spectrometer having Ar^+ laser ($\lambda = 532 \text{ nm}$) for excitation.

The near surface structure in both virgin and implanted samples was investigated by glancing angle x-ray diffraction (Cu K_α ; $\lambda = 0.154 \text{ nm}$) on a Seifert 3003 TT X-ray diffractometer. The angle of incidence between the beam and sample surface was kept at 0.1° and the diffraction patterns were recorded in the range of 14° – 30° .

Surface hardness measurements were carried out on a UHL Microhardness Tester using a Knoop indenter. Test loads from 9.8 to 98.1 mN were applied for a dwell time of 30 s. The indentation depth was calculated using the relation:

$$\text{Depth of indentation } \tau = \frac{d}{30} \mu\text{m},$$

where d is the long diagonal of the Knoop indentation mark.

III. RESULTS AND DISCUSSION

A. Estimation of implantation induced disordering

Ion beam treatment creates disordered structures within the implanted layers of polymers in the form of distorted carbon rings. The values for this disorder content in implanted polymers can be calculated from optical absorption spectra by measuring the Urbach energy (E_u) using the Urbach edge method. E_u is related to the statistical distribution of sp^2 clusters and chains of different shape and size. Therefore, the disorder content present in the polymers as a result of the lack of ordered ring structures can be evaluated in terms of Urbach energy (E_u) from the optical absorption spectra.

Figure 2 presents the UV-Visible absorption spectra of virgin and Ar^+ implanted (fluences of 5×10^{14} , 1×10^{15} , and 1×10^{16} ions cm^{-2}) CR-39 polymer. In the virgin

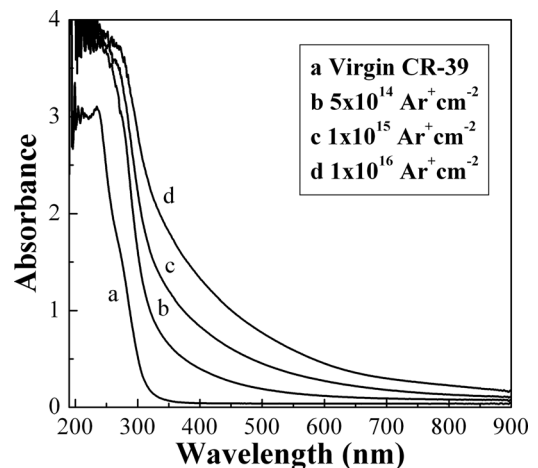


FIG. 2. UV-VIS absorption spectra of CR-39 polymer: (a) virgin, and implanted at 130 keV to (b) 5×10^{14} , (c) 1×10^{15} , and (d) 1×10^{16} Ar^+ cm^{-2} .

CR-39 sample, two absorption bands are observed at 208 and 240 nm. These bands generally arise from $n \rightarrow \pi^*$ and $\pi \rightarrow \pi^*$ transitions taking place as a result of the double bonds between carbon and oxygen with the lone pair of electrons present on oxygen.¹⁷

After Ar^+ implantation, the two bands in the virgin sample merge to one band with increased intensity and absorption spectra that shows a shift of the absorption edge from ultraviolet to the visible region. In the UV-VIS spectrum of the implanted CR-39 (Fig. 2, curves b, c, and d), the sharpness of the band edge is destroyed and as a result the edge flattens out with increasing ion fluence. The experimental data after Ar^+ implantation in Fig. 2 indicate an exponential tail extending below the bandgap edge. Ion implantation creates dangling bonds, free radicals, and saturated bonds resulting in disorder accumulation in the implanted matrix in the form of localized states between bandgap levels. These irregularities in the bandgap level of the polymers are usually depicted in terms of Urbach energy.¹⁸ The Urbach energy E_u is the width of the absorption edge and is a measure of the disorder content.¹⁹ Below the bandgap edge, the subedge exponential absorption corresponds to the Urbach edge.²⁰ The Urbach energy can be obtained by the Urbach edge method²¹ using the following equation:

$$\alpha(\nu) = \alpha_{00} \exp\left[\frac{h\nu - E_{00}}{E_u}\right], \quad (1)$$

where α is optical absorption coefficient, $h\nu$ is the energy of the incident photon corresponding to the exponential sub-edge below the bandgap edge in the absorption spectra, E_u is the Urbach energy, and E_{00} and α_{00} are fitting parameters. E_u is calculated as the reciprocal of the slope from the linear fit of a semilog plot of $\alpha(\nu)$ vs $h\nu$. All such plots for the virgin state and the different implantation doses in CR-39 (curves a, b, c, and d) have been depicted in Fig. 3.

A sharp increase in the value of Urbach energy from 0.77 eV (virgin sample) to 1.48 eV (at a fluence of $10^{16} \text{ Ar}^+ \text{ cm}^{-2}$) has been observed. As Urbach energy is a measure of disorder content,¹⁹ therefore, it can be inferred from Fig. 3

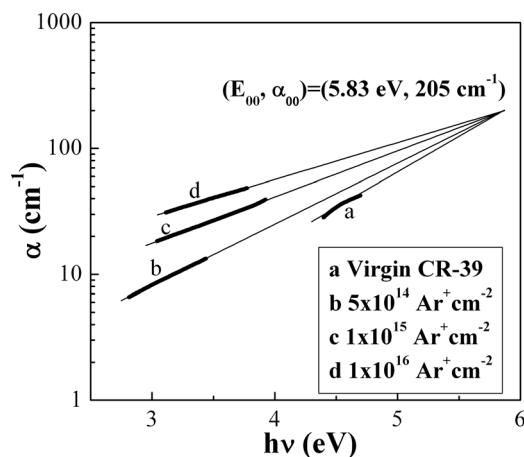


FIG. 3. Plots of $\ln(\alpha)$ vs $(h\nu)$ used to determine the Urbach energy in CR-39 polymer: (a) virgin, and implanted at 130 keV to (b) 5×10^{14} , (c) 1×10^{15} , and (d) $1 \times 10^{16} \text{ Ar}^+ \text{ cm}^{-2}$.

that disorder in the form of localized states within the band tails of electronic states is enhanced with increased ion fluence. The extrapolations to higher energy of the absorption edge data (curves a, b, c, and d in Fig. 3) converge to a focal point called the Urbach focus, described by the coordinates (E_{00}, α_{00}) .²¹ The results are shown in Fig. 3 as the solid lines and their converging point has been found to be approximately $(E_{00}, \alpha_{00}) = (5.83 \pm 0.01 \text{ eV}, 205 \text{ cm}^{-1})$. The energy corresponding to the Urbach focus seems to indicate the value of energy in a nearly disorder-free material. In the present case the disordering has been induced by varying doses of implantation and has been compared with the values corresponding to unimplanted specimens of polymer materials. The Urbach focus arises due to a mathematical result of the fact that the Urbach slope and the optical bandgap in the polymeric matrix both depend in the same way on the activity of the phonon modes.²²

To study the effect of disorder accumulation in the form of localized states within the band tails on the optical properties of implanted specimens, the optical bandgap from the UV-Visible absorption spectra has been calculated using Tauc's relation:²⁰

$$(\alpha h\nu)^{1/2} \alpha (h\nu - E_{\text{opt}}). \quad (2)$$

Here $h\nu$ is the energy of the incident photon corresponding to the fundamental absorption edge and E_{opt} is the optical bandgap. For the determination of optical bandgap, $(\alpha h\nu)^{1/2}$ was plotted as a function of photon energy ($h\nu$), taking into account the linear portion of the fundamental absorption edge of the UV-VIS spectra (curves a–d in Fig. 2). Figure 4 shows the bandgap plots of virgin and implanted (at different fluences) CR-39 polymer, and the results are presented in Table I.

A continuous decline in the bandgap with increasing ion fluence has been observed. The creation of unsaturated bonds in the implanted regions generates more delocalized π electrons,^{11,12,18} which need less energy to promote electronic transitions between these levels. As a result the absorption

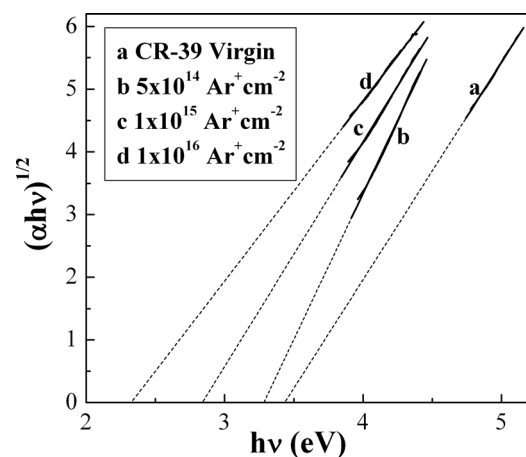


FIG. 4. Plots of $(\alpha h\nu)^{1/2}$ vs $(h\nu)$ used to determine optical bandgap in CR-39 polymer: (a) virgin, and implanted at 130 keV to (b) 5×10^{14} , (c) 1×10^{15} , and (d) $1 \times 10^{16} \text{ Ar}^+ \text{ cm}^{-2}$.

TABLE I. Variation of optical bandgap (E_{opt}), Urbach energy (E_u), number of carbon atoms per cluster (M), and number of carbon atoms per conjugation length.

Fluence (ions cm^{-2})	Optical band gap E_{opt} (eV)	Urbach energy E_u (eV)	No. of carbon atoms per cluster M	No. of carbon atoms per conjugation length N
Virgin	3.43 ± 0.03	0.77 ± 0.05	—	—
5×10^{14}	3.28 ± 0.01	0.90 ± 0.02	~ 110	~ 5
1×10^{15}	2.84 ± 0.01	1.18 ± 0.04	~ 146	~ 6
1×10^{16}	2.32 ± 0.02	1.48 ± 0.02	~ 218	~ 8

edge shifts to the longer wavelength (lower energy regions) causing the reduction in bandgap.

The dependence of optical bandgap on the disordering parameter (E_u) has been established, and results are shown in Fig. 5. A linear correlation $E_{\text{opt}} = 4.67 - 1.57 E_u$ has been obtained between the value of the Urbach energy and the optical bandgap for virgin and Ar^+ implanted CR-39 specimens, as depicted in Fig. 5. The influence of E_u is nearly 1.5 times on the value of E_{opt} in the present case of CR-39 polymer. Hence, it can be inferred from the above correlation that changes in the optical bandgap are due to the disordered structure formed by the accumulation of defect states (unsaturated bonds, dangling bonds, π electrons, etc.) on the surface of the implanted CR-39 polymer.

The visual examination of implanted specimens indicate a sharp change in color from transparent (virgin) to dark brown at the highest fluence ($1 \times 10^{16} \text{Ar}^+ \text{cm}^{-2}$). It is clear from the transmission spectra (Fig. 6, curves b, c, and d) that the transmittance gradually decreases with increasing ion dose, which can be a result of the formation of unsaturated and conjugated bonds as an effect of disordering produced on the surface of the CR-39 polymer due to Ar^+ implantation. The broken carbon-hydrogen bonds result in the formation of conjugated carbon-carbon double bonds to which surface color is sensitive. The decline in optical transmission with increasing ion dose implies growth of the carbon clusters, which are the basic absorbing centers in the implanted polymers.¹⁰ At the highest dose (Fig. 6, curve d) the UV region is almost blocked. This behavior is generally interpreted as being caused by the abrupt increase in UV absorp-

tion as a result of the formation of conjugated bonds in polymers as an effect of implantation.^{23,24} The color of organic species is mainly due to the extent of conjugation in its structure.¹⁷ Hence, changes in both the optical transmission and absorption spectra indicate enhancement in conjugated bonds in implanted specimens, which may cause the change in color of these specimens.

Furthermore, the dependence of bandgap energy on the number, type, and structural arrangement of the carbon bonds in the conjugated chain structure, or per carbonaceous cluster network—whatever is formed as an effect of implantation in CR-39 polymer—can be analyzed.²⁵ In the present case, as seen from SRIM calculations, both the electronic ($2.66 \text{eV}/\text{\AA}$) and nuclear ($2.70 \text{eV}/\text{\AA}$) energy losses are comparable, which gives equal probabilities of chain scissioning and cross-linking taking place.³ This results in the increase of conjugation length and formation of carbon clusters. The number of carbon atoms per conjugation length N can be estimated from E_{opt} values using the following relation:²⁶

$$N = \frac{2\beta\pi}{E_{\text{opt}}}. \quad (3)$$

During implantation these carbon atoms couple together and give rise to a carbonaceous network in the form of carbon clusters. The number of carbon atoms present per cluster, assuming that the structure of the cluster is like a buckminsterfullerene, i.e., C_{60} ring, in these structures can be calculated by the following formula:²⁷

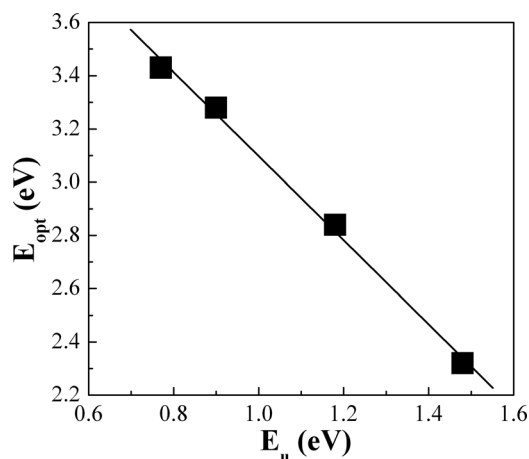


FIG. 5. Plot of Urbach's energy (E_u) vs optical bandgap (E_{opt}) values for virgin and implanted CR-39 specimens.

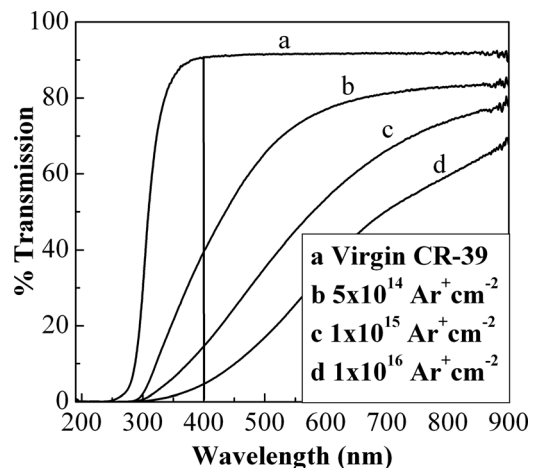


FIG. 6. UV-VIS transmission spectra of CR-39 polymer: (a) virgin, and implanted at 130 keV to (b) 5×10^{14} , (c) 1×10^{15} , and (d) $1 \times 10^{16} \text{Ar}^+ \text{cm}^{-2}$.

$$E_{\text{opt}} = \frac{34.3}{\sqrt{M}}, \quad (4)$$

where M is the number of carbon atoms per cluster. The number of carbon atoms per conjugation length and number of carbon atoms per cluster have been calculated from the above formula, and values are shown in Table I.

The determination coefficient was ~ 0.99 for all the calculations. Table I indicates an increase in the disordering parameter and conjugation length with simultaneous clustering of carbon atoms in the CR-39 polymer after ion implantation and, hence, supports the change in color and decrease in bandgap of the implanted specimens.

The virgin and implanted CR-39 specimens were further characterized using Raman spectroscopy and x-ray diffraction techniques. The results of Raman spectroscopy give additional details on damage accumulation in the implanted specimens in the form of carbon clustering, whereas the results of x-ray diffraction only detect the increase in disorder content with increasing ion fluence.

B. Evaluation of implanted/damaged layers through Raman analysis

The structure of virgin and implanted CR-39 samples was determined using the Raman spectroscopic technique. Figure 7 shows the Raman spectra of virgin and implanted CR-39 samples. Raman spectra of the virgin CR-39 sample (Fig. 7, curve a) contains several peaks at 820, 891, 961, 1032, 1130, 1292, 1461, 1644, 1744, 2913, and 2962 cm^{-1} . The highest intensity bands at 2913 and 2962 cm^{-1} are due to sp^3 C-H stretching, whereas strong intensity bands at 1032, 1130, and 1292 cm^{-1} can be attributed to the C-O-C stretching vibrations. The other strong intensity band at 1461 cm^{-1} is due to CH_3 deformation. The medium intensity bands at 820, 891, and 961 cm^{-1} originate from C-H out-

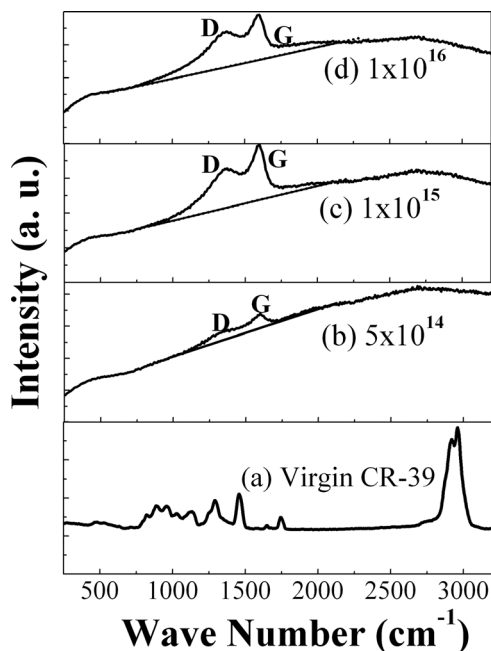


FIG. 7. Raman spectra of CR-39 polymer: (a) virgin, and implanted at 130 keV to (b) 5×10^{14} , (c) 1×10^{15} , and (d) 1×10^{16} $\text{Ar}^+ \text{cm}^{-2}$.

of-plane bending modes, while the bands appearing at 1644 and 1744 cm^{-1} mark the presence of C=C and C=O stretching.²⁸ The presence of all these bands confirms the fundamental monomer structure of the CR-39 polymer.¹¹ After argon ion implantation all these bands disappear, which indicates polymer chain scissioning. The disappearance of all these bands as a result of implantation points toward the reduction of hydrogen content and evolution of gaseous products from the surface of the CR-39 polymer.^{11,29,30}

As a result of implantation, the appearance of two bands at 1597 cm^{-1} and at 1363 cm^{-1} has been observed. These two bands are named graphitelike G and disorder D bands of the disordered carbon structure.^{11,29-32} The G band corresponds to the optically allowed E_{2g} zone center mode of graphite whereas the D peak around 1363 cm^{-1} is a breathing mode of A_{1g} symmetry involving phonons near the K zone boundary. This mode (D band) is forbidden in perfect graphite and only becomes active in the presence of disorder.³³ The G band belongs to the in-plane bond-stretching motion of pairs of C sp^2 atoms, whereas the D band is an indication that the sp^2 sites are organizing into graphitic rings.^{31,32}

All the curves of implanted spectra (curves b, c and d in Fig. 7) show a second-order Raman feature at nearly 2750 cm^{-1} which is assumed to be a counterpart of the 1363 cm^{-1} (2×1363) band.^{33,34} The appearance of this band may be due to the formation of graphitic clusters on the order of nanometers in implanted regions. Indication of strong photoluminescence (PL) can be seen from the Raman spectra of implanted specimens. This may be ascribed to the increase in defect density in the CR-39 polymer caused by the implantation of energetic particles.³⁵ This PL intensity can be predicted using the ratio of the slope of the Raman spectra to the fitted intensity of the G peak.³⁴ It is clear from Fig. 7 (curves b, c, and d) that the slope of the Raman spectra decreases with an increase in ion fluence, which points toward the reduction in PL intensity. This continuous decrease in PL intensity with increasing ion fluence may be due to the production (creation) of nonradiative recombination sites (e.g., dangling bonds) formed as a result of the decrease in hydrogen concentration on the surface of implanted specimens.³⁶ To analyze structural changes in the implanted specimens, all the Raman spectra were fitted with Gaussian following background subtraction. After deconvolution with Gaussian fit, the D and G bands were exactly separated in the spectrum (see Fig. 8). Different parameters such as positions and intensities of D and G bands were calculated from these deconvoluted curves and are given in Table II.

It is clear from Table II that the ratio of relative intensities of the D and G bands (I_D/I_G ratio) increases with increasing ion fluence. Because the D peak corresponds to an increase in the amount of unorganized carbon in the implanted specimens and a decrease in the crystallite size of graphitic zones, therefore, an increase in I_D/I_G ratio indicates enhancement in the disorder content in implanted specimens with increasing ion fluence. This result is consistent with the increase in disorder parameter (E_w) calculated from UV-VIS analysis. It is clear from Table II that the width of the D peak increases with a simultaneous decrease in the width of G

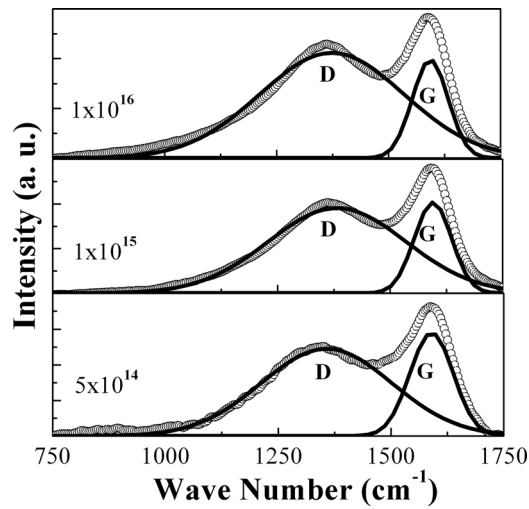


FIG. 8. Deconvoluted Raman spectra of CR-39 polymer implanted at 130 keV to 5×10^{14} , 1×10^{15} , and 1×10^{16} $\text{Ar}^+ \text{cm}^{-2}$.

peak. This indicates that more sp^2 C atoms are organizing into rings (carbon clusters) with increasing disorder.

The crystallite size L_a (in nm) of graphitic zones for disordered amorphous carbon materials can be calculated using the I_D/I_G ratio from the relation:^{34,37,38}

$$L_a = \frac{4.95}{I_D/I_G}. \quad (5)$$

The values of crystallite size calculated from the above formula are given in Table II. A continuous decline in crystallite size with increasing ion fluence has been observed. This also supports the increase in unorganized carbon with increasing ion fluence in the graphitic layers formed on the surfaces of implanted CR-39 specimens and, hence, supports enhancement in disorder content. The results of Raman analysis also point toward the formation of disordered graphitic zones on the surface of implanted specimens. Because it indicates the formation of carbon clusters in implanted regions, this study also supports the change in color and decline in bandgap of implanted samples with increasing ion fluence.

A correlation between both of the disordering parameters (E_u and I_D/I_G ratio) has been established, and results are shown in Fig. 9. A linear correlation, $E_u = 1.72 I_D/I_G - 0.41$ has been obtained between the value of the Urbach energy and the I_D/I_G ratio for Ar^+ implanted CR-39 specimens with varying doses, as depicted in Fig. 9. The dependence of optical bandgap on the disordering parameter (I_D/I_G ratio) for implanted specimens has also been established and, results

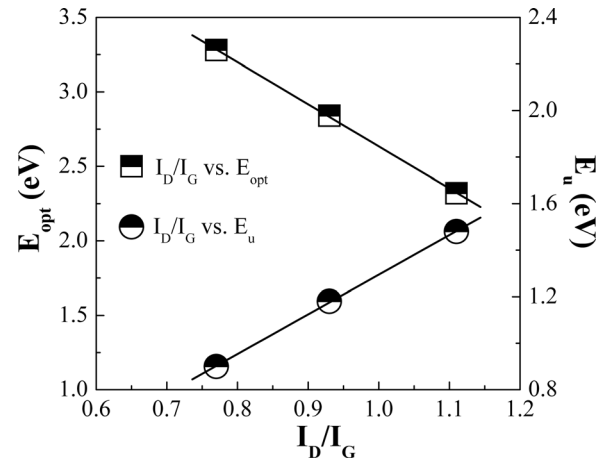


FIG. 9. Plots of I_D/I_G ratio vs optical bandgap (E_{opt}) and Urbach energy (E_u) values, respectively, for implanted CR-39 specimens at varying doses.

are shown in Fig. 9. A linear correlation $E_{\text{opt}} = 5.45 - 2.82 I_D/I_G$ has been obtained between the value of the optical bandgap and I_D/I_G ratio for Ar^+ implanted CR-39 specimens as depicted in Fig. 9. The influence of I_D/I_G ratio is nearly 1.7 times on E_u and 3 times on E_{opt} , respectively, in the present case of implanted CR-39 polymeric samples. Hence, it can be inferred from the above correlations that changes in the optical bandgap are due to the disordered graphitic structure formed by the clustering of carbon atoms on the surface of implanted CR-39 polymer.

C. Analysis of disorder accumulation by x-ray diffraction method

The study of x-ray diffraction patterns of virgin and implanted CR-39 specimens reveals the disordering present in the structure. The XRD patterns of virgin and argon implanted CR-39 samples with different fluences are shown in Fig. 10. It can be seen clearly from Fig. 10 (curve a) that the XRD spectra of the virgin CR-39 sample mainly consist of a broad peak extending from 14° – 27° and nearly centered at 20.33° . This kind of feature is generally seen in the x-ray diffraction patterns of amorphous polymers and is termed an amorphous halo.^{39–41} Therefore, the structure and shape of the diffraction pattern of the virgin CR-39 sample indicate that it is amorphous in nature. Only small changes were obtained in the XRD pattern of the implanted samples. After implantation with a dose of 10^{15} $\text{Ar}^+ \text{cm}^{-2}$, a slight decrease in the intensity of this halo (curve b) has been observed. The peak intensity of this amorphous halo further decreases with increase in ion fluence (curve c). This decline in the intensity of the amorphous halo with varying ion fluence indicates the

TABLE II. Values of position and intensity of D and G bands calculated from the deconvoluted Raman and value of crystallite size calculated from intensity ratio of D and G bands of implanted CR-39 specimens.

Sample (ions cm^{-2})	Center of D band	Center of G band	Width of D band (cm^{-1})	Width of G band (cm^{-1})	Peak Intensity of D band	Peak Intensity of G band	I_D/I_G	Crystallite size (nm)
5×10^{14}	1358	1589	263	96	1203.7	1549.7	0.77	6.43
1×10^{15}	1381	1595	295	87	1930.3	2082.1	0.93	5.32
1×10^{16}	1373	1593	323	83	4212.6	3799.9	1.11	4.46

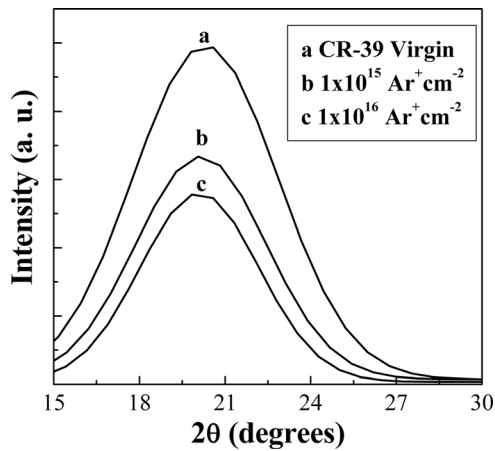


FIG. 10. GAXRD patterns of CR-39 polymer: (a) virgin, and implanted at 130 keV to (b) 10^{15} and (c) 10^{16} $\text{Ar}^+ \text{cm}^{-2}$.

enhancement in structural disorder inside the polymeric matrix as an effect of ion implantation.⁴²⁻⁴⁴

The results of XRD analysis are in agreement with enhancement in disorder parameters (E_u and I_D/I_G ratio) with increasing ion fluence.

D. Microhardness analysis

The change in Knoop microhardness with different applied loads in the CR-39 polymer due to Ar^+ implantation with increasing ion fluence is shown in Fig. 11. It is clear from Fig. 11 that Knoop microhardness number (KHN) increases with increasing ion fluence and at the highest fluence of 1×10^{16} $\text{Ar}^+ \text{cm}^{-2}$, the value of KHN becomes nearly seven times that of the virgin CR-39 polymer at the applied load of 9.8 mN. Figure 12 shows the changes in microhardness with penetration depth corresponding to different applied loads for CR-39 samples. Figure 12 (curve a) indicates that the surface hardness of the pristine CR-39 sample was almost the same up to the $2.9 \mu\text{m}$ (depth of indentation at highest load) level. But after Ar^+ implantation, Knoop microhardness varies with the depth of indentation corresponding to different applied loads and it is maximum, nearly seven times its original value, at a depth of $0.35 \mu\text{m}$ with a load of 9.8 mN for the highest ion fluence (1×10^{16} $\text{Ar}^+ \text{cm}^{-2}$). The

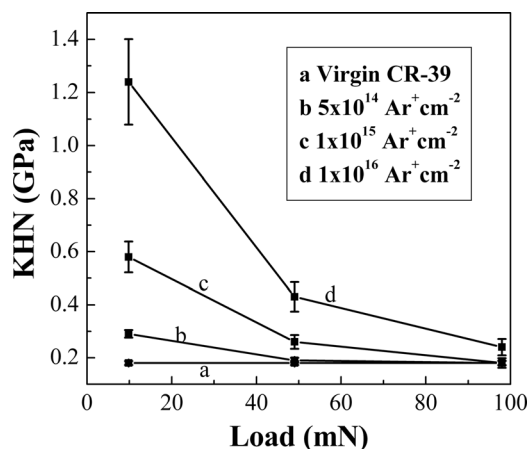


FIG. 11. Hardness-load curves of (a) virgin, and implanted at 130 keV to (b) 5×10^{14} , (c) 1×10^{15} , and (d) 1×10^{16} $\text{Ar}^+ \text{cm}^{-2}$.

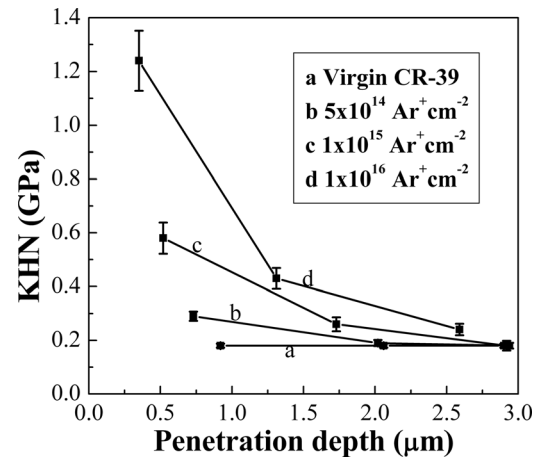


FIG. 12. Hardness-depth profile of (a) virgin, and implanted at 130 keV to (b) 5×10^{14} , (c) 1×10^{15} , and (d) 1×10^{16} $\text{Ar}^+ \text{cm}^{-2}$.

measured hardness is not the true hardness of the implanted layer itself but is given by the deformation stress of the modified surface layer. With an increase in load the depth of indentation increases and becomes more than the thickness of implantation-modified layers, causing more contribution from the substrate and, hence, lowering the hardness values nearer to the unimplanted specimen, as seen in Figs. 11 and 12.

At higher loads when the indenter penetrates beyond the implantation-modified layers, microhardness values suddenly drop as a soft cover comes in the way of the indenter. This implies that the measured hardness values at these loads are somewhat less than the value of the original modified layer.⁴ The change in hardness of implanted specimens may be due to the structural and bonding changes which are taking place inside the polymeric specimen due to ion implantation.

In the present case, the dependence of the Knoop microhardness number (KHN) at the applied load of 9.8 mN for virgin and implanted (with varying doses) CR-39 polymer on the disorder parameter E_u and the intensity ratio (I_D/I_G) of D and G bands observed in the Raman spectra, respectively, has been established, and results are presented in Fig. 13.

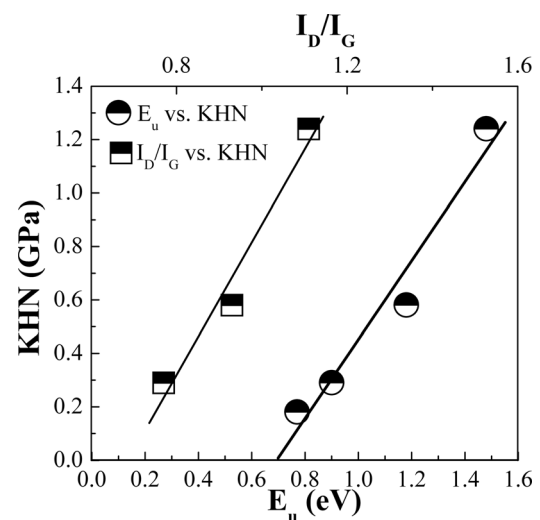


FIG. 13. Plots of Urbach energy (E_u) and I_D/I_G ratio, respectively, vs KHN (GPa) values at the applied load of 9.8 mN for virgin and implanted CR-39 polymer.

Linear correlations of the types $KHN = 1.48 E_u - 1.02$ and $KHN = 2.81 (I_D/I_G) - 1.93$, respectively, in these cases have been found, as depicted in Fig. 13. From these correlations the dependence of KHN on disordering produced due to implantation is clearly signified.

Significant effects of ion bombardment in polymers are ionization and bond breakage, leading to cross-linking, branching, chain scission accompanied by radical formation, and gas evolution.^{12–14} The main factor that plays a key role in the enhancement of the Knoop microhardness is the creation via cross links of carbon-rich clusters with disordered graphite structure in the implanted surface, which is supposed to be very hard compared with a purely graphitic structure.⁴⁵ The bathochromic shift of the absorption spectra (Fig. 2), increase in Urbach energy, and continuous reduction in the values of the optical bandgap (Table I) indicate the formation of a three-dimensional network of conjugated bonds and carbon clusters. Furthermore, the increase in the I_D/I_G ratio (Table II) gives an idea about the formation of disordered graphitelike structure having distorted carbon rings in it. X-ray diffraction also gives signs of increase in disorder in implanted specimens. Hence, the outcome of all the characterization techniques discussed in the above sections proposes the idea of the formation of disordered/distorted carbon clusters in implanted specimens and, hence, supports the increase in Knoop microhardness values with increase in Ar^+ ion fluence in the CR-39 polymer.

IV. CONCLUSIONS

The presence of disorder on the surface of Ar^+ implanted CR-39 polymer has been corroborated using UV-VIS, Raman, and x-ray diffraction techniques. A sharp increase in the value of disorder (Urbach energy) from 0.77 eV (virgin sample) to 1.48 eV (at a fluence of $10^{16} Ar^+ cm^{-2}$) has been observed using UV-VIS absorption spectroscopy. The disorder in the structure of the implanted specimens was further indicated by the appearance of disorder (D band) of amorphous carbon in the Raman spectra of implanted specimens. The linear dependence of optical bandgap (E_{opt}) with disorder content (E_u) has been observed and the influence of E_u is nearly 1.5 times on E_{opt} . Furthermore, E_{opt} correlates linearly with the I_D/I_G ratio, the influence of which is found to be nearly 3 times on it.

The increase in Knoop microhardness number (KHN) is correlated linearly with the disorder parameter E_u and the intensity ratio (I_D/I_G). These correlations clearly signify the dependence of KHN on the disordering produced due to implantation. The outcome of all the characterization techniques indicates an increase in disordering parameter and conjugation length with simultaneous clustering of carbon atoms in the CR-39 polymer after ion implantation and, hence, supports the change in properties of the implanted specimens.

ACKNOWLEDGMENTS

The authors are thankful to the Department of Science and Technology (DST), New Delhi, India, and UGC-DAE Consortium for Scientific Research, Mumbai Centre, Bhabha Atomic Research Centre, Mumbai, India, for providing kind

support. One of the authors (N.S.) is thankful to the Council of Scientific and Industrial Research, India for providing the kind financial support in the form of a Senior Research Fellowship (SRF). The authors are also thankful to Mr. Arun Kumar, Materials Science Division, IGCAR, Kalpakkam, India for his kind help during implantation.

- ¹M. Chanda and S. K. Roy, *Industrial Polymers, Specialty Polymers, and their Applications* (CRC, Taylor & Francis, Boca Raton, FL, 2009).
- ²P. A. Tres, *Designing Plastic Parts for Assembly*, 6th ed. (Hanser Gardner, Cincinnati, OH, 2006).
- ³D. Fink, *Fundamentals of Ion-Irradiated Polymers* (Springer-Verlag, Berlin, 2004).
- ⁴R. J. Rodriguez, A. Medrano, J. A. Garcia, G. G. Fuentes, R. Martinez, and J. A. Puertolas, *Surf. Coat. Technol.* **201**, 8146 (2007).
- ⁵A. Turos, A. M. Abdul-Kader, R. Ratajczak, and A. Stonert, *Vacuum* **83**, S54 (2009).
- ⁶A. M. Visco, L. Torrisi, N. Campo, and A. Picciotto, *Int. J. Polymer Anal. Char.* **15**, 73 (2010).
- ⁷A. Kondyurin and M. Bilek, *Ion Beam Treatment of Polymers, Applications Aspects from Medicine to Space*, 1st ed. (Elsevier, Amsterdam, 2008).
- ⁸E. H. Lee, *Nucl. Instr. Methods Phys. Res. B* **29**, 151 (1999).
- ⁹A. Mackova, V. Havranek, V. Svorcik, N. Djourellov, and T. Suzuki, *Nucl. Instr. Methods Phys. Res. B* **240**, 245 (2005).
- ¹⁰V. N. Popok, I. I. Azarko, and R. I. Khaibullin, *Tech. Phys.* **72**, 459 (2002).
- ¹¹T. Sharma, S. Aggarwal, A. Sharma, S. Kumar, D. Kanjilal, S. K. Deshpande, and P. S. Goyal, *J. Appl. Phys.* **102**, 063527 (2007).
- ¹²E. Yap, D. G. McCulloch, D. R. McKenzie, M. V. Swain, L. S. Wielunski, and R. A. Clissold, *J. Appl. Phys.* **83**, 3404 (1998).
- ¹³E. G. Gerstner, D. G. McCulloch, D. R. McKenzie, and E. Yap, *Philos. Mag. A* **79**, 391 (1999).
- ¹⁴L. S. Wielunski, R. A. Clissold, M. V. Swain, E. Yap, D. G. McCulloch, and D. R. McKenzie, *Nucl. Instr. Methods Phys. Res. B* **127**, 698 (1999).
- ¹⁵B. A. El-Badry, M. F. Zaki, A. M. Abdul-Kader, T. M. Hegazy, and A. A. Morsy, *Vacuum* **83**, 1138 (2009).
- ¹⁶A. M. Abdul-Kader, B. A. El-Badry, M. F. Zaki, T. M. Hegazy, and H. M. Hashem, *Philos. Mag.* **90**, 2543 (2010).
- ¹⁷D. L. Pavia, G. M. Lampman, and G. S. Kriz, *Introduction to Spectroscopy*, 2nd ed. (Harcourt, Brace, New York, 1994).
- ¹⁸A. Das, S. Dhara, and A. Patnaik, *Nucl. Instr. Methods Phys. Res. B* **149**, 53 (1999).
- ¹⁹G. Fanchini and A. Tagliaferro, *Appl. Phys. Lett.* **85**, 730 (2004).
- ²⁰J. Tauc, *Amorphous and Liquid Semiconductors* (Plenum, London, 1976).
- ²¹T. Datta, John A. Woollam, and W. Notohamiprodjo, *Phys. Rev. B* **40**, 5956 (1989).
- ²²S. R. Johnson and T. Tiedje, *J. Appl. Phys.* **78**, 5609 (1995).
- ²³I. P. Kozlov, V. B. Odzhaev, I. A. Karpovich, V. N. Popok, and D. V. Sviridov, *J. Appl. Spectrosc.* **65**, 390 (1998).
- ²⁴K. Sakamoto, M. Iwaki, and K. Takahashi, *J. Mater. Res.* **11**, 2656 (1996).
- ²⁵D. Fink, W. H. Chung, R. Klett, A. Schmoltdt, J. Cardoso, R. Montiel, M. H. Vazquez, L. Wang, F. Hosoi, H. Omichi, and P. Goppelt-Langer, *Radiat. Eff. Defects Solids* **133**, 193 (1995).
- ²⁶J. Robertson and E. P. O'Reilly, *Phys. Rev. B* **35**, 2946 (1987).
- ²⁷S. Saravanan, M.R. Anantharaman, S. Venkatachalam, and D.K. Avasthi, *Vacuum* **82**, 56 (2008).
- ²⁸D. W. Mayo, F. A. Miller, and R. W. Hannah, *Course Notes on the Interpretation of Infrared and Raman Spectra* (Wiley, New York, 2004).
- ²⁹K. G. Kostov, M. Ueda, I. H. Tan, N. F. Leite, A. F. Beloto, and G. F. Gomes, *Surf. Coat. Technol.* **186**, 287 (2004).
- ³⁰H. Watanabe and M. Iwaki, *Nucl. Instr. Methods Phys. Res. B* **206**, 1106 (2003).
- ³¹A. Das, S. Dhara, and A. Patnaik, *Phys. Rev. B* **59**, 11069 (1999).
- ³²G. R. Rao, Z. L. Wang, and E. H. Lee, *J. Mater. Res.* **8**, 927 (1992).
- ³³R. J. Nemanich and S. A. Solin, *Phys. Rev. B* **20**, 392 (1979).
- ³⁴A. C. Ferrari and J. Robertson, *Phys. Rev. B* **61**, 14095 (2000).
- ³⁵J. S. Chen, S. P. Lau, Z. Sun, B. K. Tay, G. Q. Yu, F. Y. Zhu, D. Z. Zhu, and H. J. Xu, *Surf. Coat. Technol.* **138**, 33 (2001).
- ³⁶C. Casiraghi, F. Piazza, A.C. Ferrari, D. Grambole, and J. Robertson, *Diamond Relat. Mater.* **14**, 1098 (2005).
- ³⁷W. H. Weber and R. Merlin, *Raman Scattering in Materials Science* (Springer, New York, 2002).

- ³⁸A. C. Ferrari, *Solid State Commun.* **143**, 47 (2007).
- ³⁹L. E. Alexander, *X-ray Diffraction Methods in Polymer Science* (Wiley Interscience, New York, 1969).
- ⁴⁰B. D. Cullity, *Elements of X-ray Diffraction*, 2nd ed. (Addison-Wesley, New York, 1978).
- ⁴¹H. P. Klug and L. E. Alexander, *X-ray Diffraction Procedures of Polycrystalline and Amorphous Materials*, 2nd ed. (Wiley Interscience, New York, 1974).
- ⁴²Y. Sun, Z. Zhu, Z. Wang, Y. Jin, J. Liu, M. Hou, and Q. Zhang, *Nucl. Instr. Methods Phys. Res. B* **209**, 188 (2003).
- ⁴³L. Singh and K. S. Samra, *Nucl. Instr. Methods Phys. Res. B* **263**, 458 (2007).
- ⁴⁴S. S. Guo, S. T. Lau, H. L. W. Chen, and X.-Z. Zhao, *J. Appl. Phys.* **94**, 5566 (2005).
- ⁴⁵Q. Wang, C. Wang, Z. Wang, J. Zhang, and D. He, *Appl. Phys. Lett.* **91**, 141902 (2007).